Structure-activity relationships and blood distribution of antiplasmodial aminopeptidase-1 inhibitors

Rébecca F. Déprez-Poulain, Marion Flipo, Catherine Piveteau, Florence Leroux, Sandrine Dassonneville, Isabelle Florent, Louis Maes, Paul Cos, Benoit Deprez

Structure-activity relationships and blood distribution of antiplasmodial aminopeptidase-1 inhibitors.

Rebecca Deprez-Poulain [1,2,3,*], Marion Flipo[1,2,3], Catherine Piveteau[1,2,3], Florence Leroux[1,2,3], Sandrine Dassonneville[1,2,3], Isabelle Florent[4], Louis Maes[5], Paul Cos[5], Benoit Deprez[1,2,3,*]

[1]INSERM U761 Biostructures and Drug Discovery and Faculté de Pharmacie, Univ Lille Nord de France, 3 rue du Pr Laguesse, Lille F-59000, France, [2]Institut Pasteur de Lille, IFR 142, Lille F-59021, France, [3]PRIM, Lille F-59000, France, [4]CNRS/MNHN, UMR7245, Molécules de Communication et Adaptation des Micro-organismes, Adaptation des Protozoaires à leur Environnent, F-75231 Paris, France, and [5] Laboratory of Microbiology, Parasitology & Hygiene, Faculty of Pharmaceutical, Biomedical and Veterinary Sciences, University of Antwerp, B-2020 Antwerp, Belgium.

[*] To whom correspondence should be addressed. phone, (+33) 320 964 947; fax, (+33) 320 964 709. E-mail, rebecca.deprez@univ-lille2.fr (R.D-P.); benoit.deprez@univ-lille2.fr (B.D.)

Home pages: U761, http://www.deprezlab.fr

PRIM, http://www.drugdiscoverylille.org.

Code de champ modifié

Abstract:

Malaria is severe infectious disease that causes between 655,000 and 1.2 million deaths annually. To overcome the resistance to current drugs, new biological targets are needed for drug development. Aminopeptidase M1 (*Pf*AM1), a zinc metalloprotease, has been proposed as a new drug target to fight malaria. Herein, we disclosed the structure-activity relationships of a selective family of hydroxamate *Pf*AM1 inhibitors based on the malonic template. In particular, we performed a "fluoro-scanning" around hit **1** that enlightened the key positions of the halogen for activity. The docking of the best inhibitor **2** is consistent with *in vitro* results. The stability of **2** was evaluated in microsomes, plasma and towards glutathione. The *in vivo* distribution study performed with the nanomolar hydroxamate inhibitor **2**(BDM14471) revealed that it reaches its site of action. However, it fails to kill the parasite at concentrations relevant to the enzymatic inhibitory potency, suggesting that killing the parasite remains a challenge for potent and drug-like catalytic-site binding *Pf*AM1 inhibitors. In all, this study provides important insights for the design of inhibitors of *Pf*AM1, and the validity of this target.

Keywords:

proteases, metalloenzymes, drug targets, protease inhibitors, plasmodium, antimalarial agents

Abbreviations used:
AcOEt, ethyl acetate; AUC, area-under-curve; BTFA, boron tris(trifluoroacetate); APN : Neutral Aminopeptidase; CA, carbonic anhydrase; CH_3CN, acetonitrile; DCM, dichloromethane; DIEA, diisopropylethylamine; DMF, dimethylformamide; DMSO, dimethylsulfoxide; EDCI, N-ethyl-3-(3-dimethylaminopropyl)carbodiimide; EtOH, ethanol; GSH, glutathione; HOBt, N-hydroxybenzotriazole; MeOH, methanol; PBS, phosphate buffered saline; RBC, red blood cells; RT, room temperature; SAR, structure−activity relationship; TEA, triethylamine; TFA, trifluoroacetic acid; THF, tetrahydrofuran; TIS, triisopropylsilane; Trt, trityl.

INTRODUCTION

The WHO/TDR initiative promotes drug target validation for neglected diseases [1]. As such, innovative strategies are being developed to discover new antiplasmodial targets and may include a target-driven approach by cell-based screening [2], drug repositioning and chemogenomics [3,4]. In this context, the *Plasmodium* proteases are putative targets [5-8]. Their study benefits from the successful work done on proteases in other pathologies, such as AIDS, hypertension and type-II diabetes [9, 10]. Among the metalloproteases of *Plasmodium*, falcilysin is involved in the intravacuolar digestion of globin and has no reported inhibitor [11]. On the other hand, aminopeptidases degrading oligopeptides resulting from haemoglobin digestion are well-studied [12-14]. Recently, inhibitors of LAP (Leucine-aminopeptidase), a hexameric aminopeptidase of the M17-family, have been described [15, 16].

Florent *et al* characterized the aminopeptidase M1 (*Pf*AM1 or *Pf*M1AAP) that shows a strict aminopeptidase activity at pH 7.4 and a broad substrate spectrum [17, 18]. *Pf*AM1 localizes differently in trophozoites and schizonts, suggesting a particular role in the intraerythrocytic life of the parasite. *Pf*AM1 degrades oligopeptides resulting from haemoglobin digestion either in the vacuole [19] or the cytosol [20]. The inhibition of *Pf*AM1 by bestatin analogues induces swollen digestive vacuoles due to the accumulation of oligopeptides [21]. Also, a role in the reinvasion of erythrocytes has been found, in agreement with the observation of Kitjaroenthan *et al* [22]. Studies on *Pf*AM1 localization suggest that it is trafficked via the parasitophorous vacuole [23]. *Pf*AM1 is also present in the nucleus, but so far no function can be related to its nuclear localization [19].

Given these results, *Pf*AM1 can be considered an attractive candidate to initiate screening and lead optimization. Our research group was the first to describe *Pf*AM1 screening and the first two series of hydroxamic non-peptidic non-selective *Pf*AM1 inhibitors with a mixed mode of action [24]. The screening of a focused library of zinc-binding molecules

[25] resulted in a malono-hydroxamic druggable hit, **1** [26]. Chemical modifications explored the introduction of steric constrains at the malonic position and led to the discovery of **2**, a nanomolar selective inhibitor of *Pf*AM1. **2** shows good physico-chemical, *in vitro* plasma stability and promising antiplasmodial activity *in vitro* [26]. Other inhibitors, such as phosphonopeptides, were subsequently published [27, 28] and were designed as mixed inhibitors of the aminopeptidases of the M1 and M17 families. The binding of one non-selective compound to *Pf*AM1 was assessed by co-crystallisation with the recombinant enzyme whose X-ray structure had been published [29]. Recently, peptide-based bestatin analogues were also disclosed [28].

This paper reports the further optimization of our inhibitors whereby initial medicinal chemistry experiments revealed that the introduction of a fluorine on the scaffold had a significant impact on the inhibitory activity [26]. First, the effect on potency of systematic moving of fluorine ("fluorine scanning") [30,31] around compounds **1** and **2** was evaluated. Also substitution at the malonic carbon and the introduction of a pyridine to introduce a positive charge, which is a hallmark of many antiplasmodials, were explored. Analogues on *Pf*AM1 covering a 2.5 log range of IC_{50}s were tested *in vitro* on the intraerythrocytic cycle. We analyze these results in the light of structure-activity relationships on the isolated enzyme and distribution/stability data of the most active *Pf*AM1 inhibitor.

RESULTS AND DISCUSSION

Synthesis of inhibitors 1-14

Inhibitors were synthesized as described in schemes 1 and 2. Precursors **5a-b,d-e** and **1-4**,**12** were synthesized as previously described [26,32]. **5c** was synthesized by a Knoevenagel reaction between 4-fluorobenzaldehyde and ethyl *N*-tert-butoxymalonamate in refluxed ethanol in the presence of piperidine. The resulting ester was saponified to give carboxylic acid **5c** as a single E-isomer as determined by ROESY NMR.

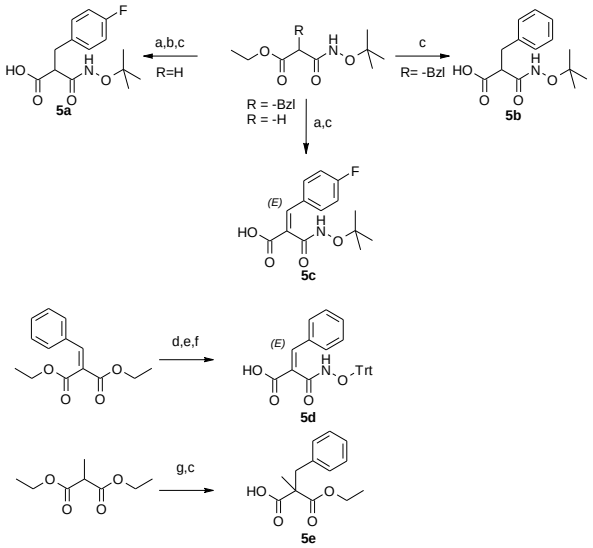

Scheme 1. Synthesis of carboxylic acid precursors **5a-e**.

(a) *para*fluoro-benzaldehyde, piperidine, abs. EtOH, reflux, 3.5 h; (b) $NaBH_3CN$, CH_3CN, 24 h, room temp.; (c) KOH, abs. EtOH, overnight, room temp.; (d) 1 eq. LiOH, THF, H_2O, 4 h, room temp.; (e) i. 1.2 eq. oxalylchloride, DCM, cat. DMF, 45 min., 0 °C; ii. 3 eq DIEA, 0.85 eq. O-tritylhydroxylamine, DCM, 0 °C then room temp., 3 h; (f) 4 eq. LiOH, THF, H_2O, overnight, room temp.; (g) i. EtONa, EtOH, 1 h , 50 °C, ii. benzylbromide, 2 h, 50 °C.

5a-d reacted with the corresponding amine after activation of the carboxylic acid function using either ethylchloroformate or EDCI/HOBt. The deprotection of the hydroxamate was performed in acidic conditions to give compounds **6-11**,**13-14**.

Compound **12** was obtained from 5**e** by coupling first the 4-fluorobenzylamine. Then, the ester was saponified, and the resulting carboxylic acid was activated and reacted with trityle-protected hydroxylamine. The final deprotection was performed in TFA/DCM.

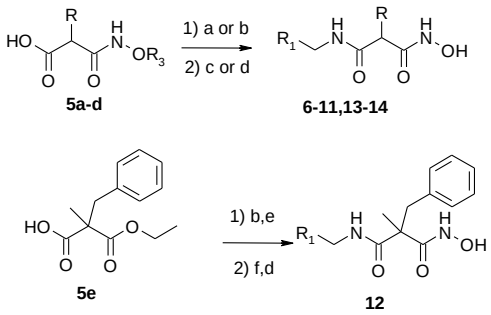

Scheme 2. Synthesis of *PfAM1* inhibitors **6-14**.

(a) i. 1.1 eq. ethylchloroformate, 1.1 eq. TEA, DCM, 30 min., 0 °C; ii. 1.1 eq. R_1-CH_2-NH_2, 1h, room temp.; (b) R_1-CH_2-NH_2, EDCI/HOBt, DMF/DIEA, 5 h, room temp. (c) BTFA (0.75 M/TFA; 25 eq.) with 0.4% H_2O, room temp. for t-butyle; (d) TFA 2%/DCM, TIS, 10 min, room temp. for trityle; (e) KOH, EtOH abs., overnight, room temp., (f) i. 1.1 eq. ethylchloroformate, 1.1 eq. TEA, DCM, 30 min., 0 °C; ii. 1.1 eq. H_2N-OTrt. HCl, 1 h, room temp.

***Pf*AM1 inhibition and selectivity towards *p*APN.**

In these series, hit **1** (IC_{50} = 27 nM) and its analogue **2** (IC_{50} = 6 nM) bearing a *p*-fluorobenzene ring were more active than **4** (IC_{50} =125 nM) deprived of a halogen (Table 1).[26] Fluorine is often used in medicinal chemistry [33-35] as it is sterically small and most often chemically inert. It is the most electronegative halogen and forms stable bonds with carbon which are poorly polarizable. Compounds **6-8**, resulting from "fluorine scanning", display a

ten-fold decrease in potency. This illustrates the importance of the presence of fluorine in the para-position of the benzylamido moiety rather than in ortho- or meta- position or on the other phenyl ring. Interestingly, compound **9** that has a fluorine atom at this critical position, and an additional fluorine, is less active than compound **1**. This finding suggests that fluorine on the benzyl malonyl moiety is exposed to a fluorophobic region. The same trend is observed for unsaturated compounds **10** and **11**, analogues of **2** (IC_{50} = 6 nM), that are seven- to ten-fold less potent. Nevertheless, the beneficial unsaturation compensates for bad fluorine position.

Substitution of a hydrogen atom by a methyl group on the malonic carbon of **1** (compound **12**) induced a two-fold loss in activity, while the substitution of para-fluorophenyl by a pyridine ring [36] in compounds **1** and **2** enabled the exploration of the properties of the enzyme pocket and generated a positive charge. Compounds **13** and **14** were about 50 times less active than their analogue.

All compounds were shown to be selective for the parasitic enzyme versus the mammalian enzyme APN (neutral aminopeptidase). The highest selectivity ratios were observed for compounds **2** and **11**.

Table 1. Inhibition of *Pf*AM1, *p*APN by compounds **1-3**, **5-13**.

Compound	Structure	*Pf*AM1 inhibition IC_{50} (nM)[a,c]	*p*APN inhibition IC_{50} (nM)[b,c]
1	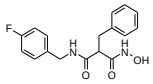	27	3616
2(BDM14471)	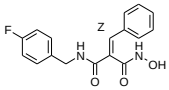	6	1372
3	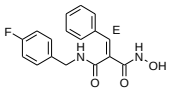	330	>10000
4	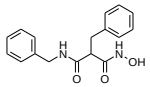	125	>10000
6	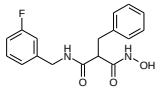	210	2333
7	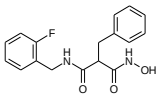	256	2223
8	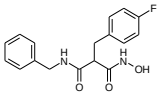	310	1324
9	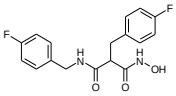	258	3956
10	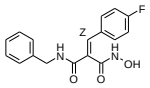	69	2400
11	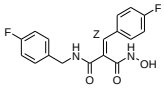	43	4200
12	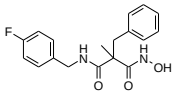	56	>10000
13	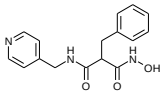	1050	4550
14	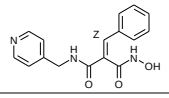	440	2000

[a] IC_{50} bestatine (nM) : 284 ; [b] IC_{50} bestatine (nM) : 2700 ; [c] mean of 3 experiments , standard error below 10% ;

To rationalize structure-activity relationships, compound **2** was docked in *Pf*AM1 (using enzyme in PDB: 3T8V) (Figure 1). The hydroxamate moiety binds the Zn^{2+} ion and is involved in a hydrogen-bond with Glu497. The S1 pocket of the enzyme is hydrophobic and able to undergo major conformational changes upon ligand binding [28]. It is characterized by hydrophobic residues (Gln317, Val459, Met462, Glu572, Tyr575, Met1034) [29] that can accommodate the benzylmalonyl substituent of **2** or larger substituents [26]. The introduction of a fluorine atom at this position, although tolerated, is not critical for activity (compound **1** vs **8** and **9**, Table 1). Interestingly, a T-staking [37, 38] between Tyr575 and phenylmeth-(Z)-ylidene moeity is observed (Figure 1), explaining why the Z isomer (**2**) is more active than the E isomer (**3**).

The amide function is engaged in two hydrogen bonds with Gly460 and Ala461 backbones. The S'1 pocket is also delimited with hydrophobic residues (Thr492, Val493 and Val 523) [29]. Although a cation-π interaction is observed between the benzyl group of **2** and Arg489, the introduction of the electron-withdrawing fluorine has a positive impact on activity (**2** vs **4**, Table 1). This may be the result of an increased desolvation entropy upon binding in this pocket. Also, the presence of the positively charged Arg489 explains why pyridine is less tolerated on that position (compounds **13-14**, Table 1).

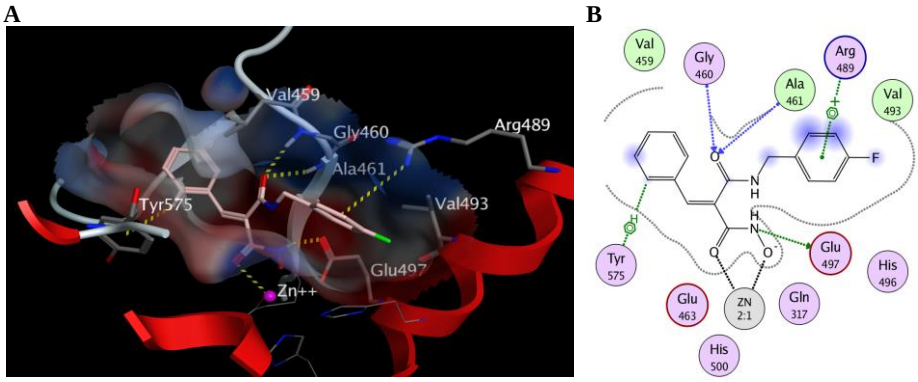

Figure 1. Binding of **2** in *PfAM1*.

(A) Docking of **2** in the enzyme (PDBcode : 3T8V). Zinc ion is colored magenta. The atoms oxygen, nitrogen are colored red and blue respectively, fluorine is colored green and carbon is shown in light pink or light gray for respectively **2** or key residues of *PfAM1*. Specific hydrogens are colored white. (B) Schematic representation of the interactions of **2** with *PfAM1*, featuring the 3-letter code of amino-acids lining the binding pocket. Polar residues are pink (blue circles for positively charged, red circles for negatively charged), apolar residues are green. Metal contacts are represented as black dotted lines. Hydrogen bonds in blue (acceptor) or green (donor) arrows respectively, Arene-H and arene-positive charge are represented as green dotted lines.

Parasite growth inhibition and cytotoxicity: None of the compounds tested was cytotoxic for MRC5 cells (IC_{50} values >32 µM, Table 2). Compounds **1**,**2**,**6-9**,**11-12** inhibited parasite growth at IC_{50}-values ranging between 11 to 50 µM (Table 2) which is comparable to other *Pf*AM1-selective or mixed *Pf*AM1/LAP inhibitors [12, 16, 27, 29] or bestatine analogues [28]. However there is a lack of correlation between enzymatic and parasite activities. Compounds very similar in structure, yet displaying low nanomolar to micromolar potencies on the enzymatic assay, show all poor activity on the parasite (*ie*. **6** vs **1**; **10** vs **8**).

Table 2. Inhibition of parasite growth by compounds **1**, **2**, **6-9**, **11-13, 15.**

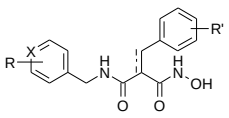

1,2,6-9,11-13

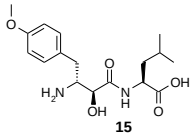

15

Compound	*Pf*AM1 [a] inhibition IC_{50} (nM)	Parasite growth [b] IC_{50} (µM)	Cytotoxicity IC_{50} (µM)
1	27	17.4 (59[f])	> 64.0
2	6	11.0 (24[f])	32.0
6	210	24.7	> 64.0
7	256	37.9	> 64.0
8	310	36.5	> 64.0
9	258	41.6	> 64.0
11	43	30.4	32.2
12	56	50.1	> 64.0
13	1050	> 64.0	> 64.0
bestatine[d]	478[e]	8-21[g]	–[c]
hPheP[CH_2]Phe[d]	79[e]	24-62[g]	–[c]
15[d]	43[e]	6.4[g]	–[c]

[a] native enzyme; [b] Mean of at least three experiments, K1 strain, IC_{50} chloroquine (nM): 154; [c] not determined; [d] reference 28 or 29; [e] recombinant enzyme; [f] FcB1 strain IC_{50} chloroquine (nM): 110; [g] 3D7 strain IC_{50} chloroquine (nM): 10.

To elucidate this large activity gap and the lack of correlation between the *in vitro* inhibition of *Pf*AM1 and the parasite growth inhibition, *in vitro* ADME parameters were explored for a set of analogues to select a compound for *in vivo* pharmacokinetics.

***in vitro* ADME parameters for 2.** Some key physicochemical parameters were measured for the most potent and selective compounds **1**, **2** and **11** (Table 3). Compounds **1**,**2** have comparable solubilities and LogD while **11** is slightly more hydrophobic and less soluble. All three compounds are stable in human plasma but compound **2** is by far the most stable compound in rodent plasma which is critical for *in vivo* pharmacokinetics. These stabilities are coherent with previous data on hydroxamate stabilities [32].

Table 3. Solubility, LogD and plasma stabilities for **1**,**2**,**11**.

Compound	Solubility (µM)[a]	LogD (pH 7.4)[a]	Rat plasma stability (h)[b]	Human plasma stability (h)[b]
1	>200	1.2	0.8	> 24
2	198	1.1	22	> 24
11	190	1.7	3.0	> 24

[a] : Solubility and LogD are measured from a DMSO stock solution; [b] : Half-life plasma stability at 37 °C using LC-MSMS (MRM detection mode).

Before the pharmacokinetic evaluation in mice, **2** was further characterized *in vitro*. **2** displays a Michael acceptor function that may be sensitive to soft nucleophiles like thiols. An *in vitro* glutathione alkylation study [39] revealed that compound **2** is isomerized *in vitro* in its (E)-isomer **3** through the GSH-adducts production (Z/E : 54/46, after 24 hours). The proportion of combined GSH-adducts of the two unsaturated isomers reaches 50% at 24 hours. **2** was also tested *in vitro* for mouse microsomal stability and was found to be very stable in a classic 30-minute assay. Interestingly, this stability was observed for both the oxidative and the non-

oxidative metabolism, suggesting that no hydrolysis of the hydroxamate moiety occurs through esterase activity.

Pharmacokinetics of 2 in mice: Female CD1 mice received **2** at 50 mg/kg intraperitoneally to evaluate whether it would be concentrated enough for *in vivo* activity against *P. berghei* infection. As the parasite is located in erythrocytes, both the plasma concentration and the distribution in erythrocytes were investigated. **2** was formulated in 50/50 DMSO/PBS at 10 mg/mL. Blood was collected at regular time intervals after dosing (Figure 2). Plasma and red blood cells (RBCs) were fractionated and quantification of **2** was performed using LC/MSMS.

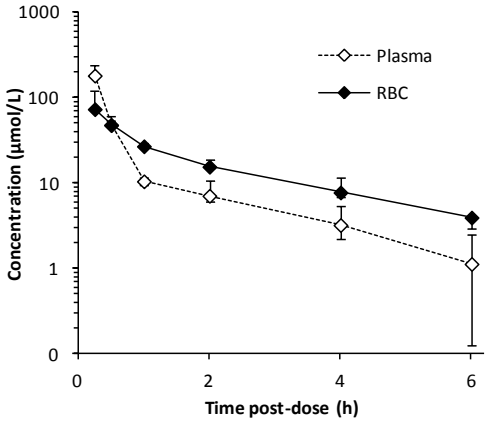

Figure 2. Concentration-time profile for compound **2**.

Concentrations in plasma (◇) or red blood cells (◆) found in female CD1 mice receiving single IP administration at 50 mg/kg. Symbols represent averages from two mice. Plasma and red blood cell data are presented as µmol/L.

Following a single dose, **2** could be measured readily after dosing and until the end of the experiment (six hours post-dose) (Figure 2), showing a plasma elimination half-life of one hour (from 1 to 6 h.; Table 4). As expected from the stability studies, only traces of carboxylic acid were formed, indicating that the hydroxamate was not a primary site of metabolism. Fortunately, as opposed to *in vitro* results, no GSH-mediated isomerisation occurred in mice

as E isomer **3** was not detected in the *in vivo* experiment either in plasma or in red blood cells. **2** penetrates red blood cells with a significant $AUC_{0\rightarrow\infty}$ of 98 µmol * h/L measured in red cells (Figure 2, Table 4).

Table 4. Pharmacokinetic parameters of **2** in female mice.

Matrix	Dose (mg/kg IP)	t_{last} (h)	$AUC_{0\rightarrow last}$ (µmol * h/L)	$AUC_{0\rightarrow\infty}$ (µmol * h/L)	$t_{1/2}$ (h)
	1*50	6			
plasma			66	68	1.0
RBCs			90	98	1.5

The global AUC for **2** in red blood cells is even higher than that in plasma suggesting that **2** enters and accumulates in RBCs. Thus the gap between *in vitro* and *in vivo* activity could not be explained by a lack of host cell penetration. However, it could possibly be explained by the trapping of the compound by a component of red blood cells before it is able to reach the parasite. It is known that Zn^{2+} ion ligands, such as dorzolamide, can be trapped in RBC by carbonic anhydrase [40]. Carbonic anhydrase is a zinc metallohydrolase that is located in red blood cells in high concentrations (150 µM total isoforms). Nevertheless, **2** does not inhibit *h*CAII (0% inhibition at 10 µM and 50 µM, tested in duplicate), indicating that it does not bind carbonic anhydrase and likely is free to enter the parasitic cell from the cytoplasm of red blood cells. In all, this shows that the gap between enzymatic inhibitory potency and antiplasmodial activity cannot be explained by any of the molecular properties of **2** tested by us.

CONCLUSION

Based on literature data, *Pf*AM1 has been regarded as essential to the malaria parasite. However, none of its described inhibitors, including ours, was able to kill the parasite at

concentrations below 1 µM, raising the question of the pharmacological relevance of inhibiting *Pf*AM1 to treat malaria. To formulate a conclusion, we must take into account that the pharmacological activity of an inhibitor is not only determined by its binding to the target and its inhibitory potency, but also by its ability to reach the target at a sufficient concentration for a sufficient period of time. The lack of pharmacokinetic data on inhibitors reported earlier made it difficult to interpret their poor antiplasmodial potency. In this paper, we report the first structurally homogeneous family of inhibitors demonstrating a 100-fold range of enzyme potency, together with antiplasmodial activities and key pharmacokinetic parameters.

Structure-activity relationships established by "fluorine scanning" showed that best position for fluorine is in para of the benzylamido group. Substitution at the malonic carbon is tolerated whereas introduction of a pyridine is deleterious for activity. The range of compounds tested here spanned a 2.5 log scale of inhibitory potency on the isolated enzyme. However, in this population, we were not able to observe any correlation between enzymatic potency and antimalarial activity. To rule out potential compound-related issues in the course of the validation of *Pf*AM1 as a drug target, we performed stability and distribution studies with **2** (BDM14471), our most promising inhibitor, taking into account potency, physico-chemical parameters and metabolic stability. Pharmacokinetic experiments in mice evidenced a significant distribution of **2** in plasma and red blood cells until 6 hours after dosing. In this experiment, **2** reached micromolar concentrations within the red blood cells that harbour the parasites in culture. Altogether, these results show that the compound reaches the site of action but fails to kill the parasite at concentrations relevant to the enzymatic inhibitory potency, suggesting that killing the parasite remains a challenge for potent and drug-like catalytic-site binding *Pf*AM1 inhibitors. A working hypothesis to explain these results could be that the catalytic activity of the *Pf*AM1 is not critical for the survival of the parasite at the

intra-erythrocyte stage. In this situation, other non-proteolytic regulatory functions of *Pf*AM1 may have to be targeted to produce antimalarial drug candidates.

MATERIALS AND METHODS

General chemistry. ^{1}H NMR and ^{13}C NMR were recorded at room temperature on a Bruker™ DPX 300 at 300 and 75 MHz, respectively. Chemical shifts are in parts per million (ppm). The assignments were made using one dimensional (1D) ^{1}H and ^{13}C spectra or two-dimensional (2D) HSQC and COSY spectra. Mass spectra were recorded on a LCMS system (Waters). HPLC analysis were performed using a C_{18} TSK-GEL Super ODS 2 µm particle size column, dimensions 50 * 4.6 mm. LCMS gradient starting from 100% H_2O / 0.1% formic acid and reaching 20% H_2O / 80% MeOH / 0.08% formic acid within 5 min at a flow rate of 1 mL/min was used. Purity (%) was determined by reversed-phase chromatography HPLC using UV detection (215 nm) , and all compounds showed purities greater than 95%. All commercial reagents and solvents were used without further purification.

Coupling reactions for amide bond formation: a) Carboxylic acid (0.66 mmol; 1 eq.) was dissolved in DCM (7 mL) and TEA (102 µL; 0.73 mmol; 1.1 eq.) was added. The mixture was cooled at 0 °C (ice bath) and ethylchloroformate (70 µL; 0.73 mmol; 1.1 eq.) was added dropwise. The reaction mixture was stirred 30 min. at 0 °C, then the desired amine (0.73 mmol; 1.1 eq.) was added. The organic layer was stirred 1h at room temperature and then evaporated. The crude product was dissolved in ethyl acetate, washed twice with aq. $NaHCO_3$ 5%, once with water and once with aq. NaCl, dried over $MgSO_4$, filtered and evaporated. The product was purified by thick layer chromatography (DCM 100%) and/or precipitated in petroleum ether (40-60) to give the expected amide. Or b) Carboxylic acid (0.1M/DMF; 1 eq.), DIEA (2.4 eq), EDCI (1.1 eq.) and HOBt (1.1 eq.) were stirred 5 min at room temperature. Then the appropriate amine (0.1 M/DMF; 1 eq) and DIEA (2 eq.) were added. The mixture was stirred 5 h at room temperature and then solvents were removed

under reduced pressure. The residue was dissolved in AcOEt and the organic phase was washed with aqueous $NaHCO_3$ 5% (6 times) and NaCl (once). The organic layer was dried over $MgSO_4$ and evaporated under reduced pressure. The residue was precipitated in petroleum ether.

Tert-butyl deprotection. Tert-butylated intermediate was dissolved in a suspension of BTFA (0.75 M/TFA; 25 eq.) with 0.4% H_2O. The reaction mixture was stirred 4 h to 5.5 h at room temp. Solvents were removed under reduced pressure and the residue was dissolved in water. The aqueous phase was basified with NaOH 1 M to pH = 7 and extracted three times with AcOEt. The organics layers were dried over $MgSO_4$, filtered and evaporated. The residue was precipitated in ether-pentane. Yields given are those of the deprotection step.

Trityl deprotection. Tritylated intermediate was dissolved in TFA 2%/DCM and triisopropylsilane was added drop by drop until the yellow color disappeared. The reaction mixture was stirred 5 min. at room temperature, solvents were removed under reduced pressure and the residue was washed with ether-pentane. Yields given are those of the deprotection step.

(E)-2-*tert*-butoxycarbamoyl-3-(4-fluorophenyl)-acrylic acid (5c). 4-fluorobenzaldehyde (32.0 mmol; 1 eq.) was added to a solution of ethyl N-*tert*-butoxy-malonate (7.163 g; 35.2 mmol; 1.1 eq.) and piperidine (1 mL) in abs. ethanol (150 mL). The solution is refluxed 3.5 h and solvent is removed under reduced pressure. The crude product is purified by flash chromatography (DCM/MeOH 98/2) to give ethyl (Z/E) 2-*tert*-butoxycarbamoyl-3-(4-fluorophenyl)-acrylate in 71% yield; purity 85%; NMR ^1H ($CDCl_3$) δ ppm : 1.21-1.29 (m; 12H); 4.24 (q; J = 7.1 Hz ; 2H); 7.01 (t; J = 8.6 Hz; 2H); 7.51-7.55 (m; 2H); 7.69 (s; 1H); 7.86 (s; NH); MS $(MH)^+$ *m/z* 310; MS $(MNa)^+$ *m/z* 332. The later ethyl ester (3.478 g, 11.25 mmol) is dissolved in abs. ethanol (115 mL) and KOH (2.57 g; 45 mmol; 4 eq.) is added. The mixture is stirred overnight at room temperature and then evaporated. The

crude product is dissolved in water. The aqueous phase is acidified with aq.HCl 1 N until pH = 1, then the carboxylic acid is extracted with ethylacetate (4*20 mL). The organic layers are pooled, dried over $MgSO_4$ and evaported to give **5c** as a yellow powder in 92% yield; Purity 95%; NMR ^{1}H (DMSO-d_6) δ ppm : 1.17 (s; 9H); 7.28 (t; *J* = 8.9 Hz; 2H); 7.61 (s, 1H); 7.64-7.69 (m; 2H); 10.83 (s; NH); 12.85 (s, OH); $t_{R\ LCMS}$ 4.19 min; MS $(MH)^+$ *m/z* 282; mp 188-190 °C.

2-Benzyl-N-(4-fluoro-benzyl)-N'-hydroxy-malonamide (1). White powder; Yield 88%; Purity 100%; NMR ^{1}H DMSO-d6 δ ppm : 2.96-3.10 (m, 2H), 3.35-3.40 (m, 1H), 4.16 (dd, *J* = 15, *J* = 5.7 Hz, 1H), 4.27 (dd, *J* = 15, *J* = 6 Hz, 1H), 7.04-7.27 (m, 9H), 8.40 (t, *J* = 5.6 Hz, NHCO), 8.93 (s, OH), 10.58 (s, CONHO); NMR ^{13}C DMSO-d_6 δ ppm : 35.0; 42.1; 52.5; 115.5 (d, J_{CF} = 21.1Hz); 126.8; 128.8; 129.4; 129.5 (d, J_{CF} = 8.4 Hz); 136.0 (d, J_{CF} = 2.3Hz); 139.6; 161.7 (d, J_{CF} = 240.4Hz); 166.3; 168.9. tr_{LCMS} 4.31 min; MS $(MH)^+$ *m/z* 317; mp 193-194 °C.

***N*-(4-Fluoro-benzyl)-*N*'-hydroxy-2-[1-phenyl-meth-(Z)-ylidene]-malonamide (2).** White powder; Yield 37% (overall); Purity 99%; NMR ^{1}H DMSO-d6 δ ppm : 4.37 (d, *J* = 6.0 Hz, 2H), 7.12-7.18 (m, 2H); 7.32-7.40 (m, 5H), 7.43 (s; 1H); 7.51-7.54 (m, 2H); 8.26 (t, *J* = 6.0 Hz, NHCO), 9.13 (s, OH), 11.01 (s, CONHO); NMR ^{13}C DMSO-d_6 δ ppm : 42.6; 115.6 (d, J_{CF} = 21 Hz); 129.3; 129.5; 129.9; 130.1; 130.6; 134.2; 136.2; 137.3; 161.8 (d, J_{CF} = 246 Hz); 163.5; 164.6. tr_{LCMS} 4.23 min; MS $(MH)^+$ *m/z* 315.

***N*-(4-Fluoro-benzyl)-*N*'-hydroxy-2-[1-phenyl-meth-(E)-ylidene]-malonamide (3).** White powder; Yield 50% (overall); Purity 99%; NMR ^{1}H DMSO-d6 δ ppm : 4.30 (d, *J* = 6.0 Hz, 2H), 7.08-7.37 (m, 10H); 8.86 (t, *J* = 6.0 Hz, NHCO), 9.08 (br s, OH), 10.70 (br s, CONHO); NMR ^{13}C DMSO-d_6 δ ppm : 42.3; 115.3 (d, J_{CF} = 20 Hz); 128.9; 129.5; 129.6; 129.8; 130.3 (d, J_{CF} = 12 Hz); 132.0; 134.3; 135.2; 161.4 (d, J_{CF} = 225 Hz); 163.3; 166.2. tr_{LCMS} 4.41 min; MS $(MH)^+$ *m/z* 315.

2*N*-Dibenzyl-*N′*-hydroxy-malonamide (4): White powder; yield 84%; purity 100%; ^{1}H NMR DMSO-*d*6 δ 3.00-3.08 (m, 2H), 3.30 (t, *J* = 6.75 Hz, 1H), 4.20 (dd, *J* = 5.1 Hz, *J* = 15 Hz, 1H), 4.30 (dd, *J* = 5.4 Hz, *J* =15 Hz, 1H), 7.10-7.23 (m, 10H), 8.20-8.23 (m, NHCO), 10.44 (s, CONHO); ^{13}C NMR (DMSO-*d*6) δ 35.1, 42.7, 52.7, 126.6, 127.1, 127.5, 128.6, 128.7, 129.3, 139.4, 139.6, 166.2, 168.6; tr_{LCMS} 4.25 min; MS $(MH)^{+}$ *m*/*z* 299; mp 167-169 °C.

2-Benzyl-*N*-(3-fluoro-benzyl)-*N′*-hydroxy-malonamide (6). White powder; Yield 90%; Purity 100%; NMR ^{1}H DMSO-d6 δ ppm : 2.98-3.12 (m; 2H); 3.29-3.35 (m; 1H); 4.21 (dd; *J* = 15.6 Hz; *J* = 6.0 Hz; 1H); 4.30 (dd; *J* = 15.6 Hz; *J* = 6.3 Hz; 1H); 6.93-7.06 (m; 3H); 7.18-7.33 (m; 6H); 8.31 (t; *J* = 6.0 Hz; NH); 8.95 (s; OH); 10.49 (s; CONHO); . tr_{LCMS} 4.51 min; MS $(MH)^{+}$ *m/z* 317; mp 167.5-168.8 °C.

2-Benzyl-*N*-(2-fluoro-benzyl)-*N′*-hydroxy-malonamide (7). White powder; Yield 70%; Purity 100%; NMR ^{1}H (DMSO-d_6) δ ppm : 3.03-3.07 (m; 2H); 3.30-3.35 (m; 1H); 4.23 (dd; *J* = 15.6 Hz; *J* = 5.6 Hz; 1H); 4.32 (dd; *J* = 15.6 Hz; *J* = 6.0 Hz; 1H); 7.02-7.32 (m; 9H); 8.25 (t; *J* = 5.7 Hz; NH); 8.95 (s; OH); 10.47 (s; CONHO); $t_{R\ LCMS}$ 4.20 min; MS $(MH)^{+}$ *m/z* 317; mp 182.3-184.7 °C.

***N*-Benzyl-2-(4-fluoro-benzyl)-*N′*-hydroxy-malonamide (8).** White powder; Yield 23%; Purity 95%; NMR ^{1}H (DMSO-d_6) δ ppm : 3.01-3.05 (m; 2H); 3.28 (t; *J* = 7.8 Hz; 1H); 4.18 (dd, *J* = 5.4 Hz, *J* = 15.3 Hz, 1H), 4.29 (dd, *J* = 6.0 Hz, *J* = 15.3 Hz, 1H), 7.04-7.11 (m; 4H); 7.19-7.29 (m; 5H), 8.24 (t, *J* = 6.0 Hz, NHCO); 8.95 (s, 1H, OH); 10.46 (s; CONHO); $t_{R\ LCMS}$ 4.36 min; MS $(MH)^{+}$ *m/z* 317.

2,*N*-Bis-(4-fluoro-benzyl)-*N′*-hydroxy-malonamide (9). Beige powder; Yield 21%; Purity 96%; NMR ^{1}H (DMSO-d_6) δ ppm : 3.00-3.04 (m; 2H); 3.26 (t; *J* = 7.8 Hz; 1H); 4.16 (dd; *J* = 5.7 Hz; *J* = 15.0 Hz; 1H); 4.26 (dd; *J* = 6.0 Hz; *J* = 15.0 Hz; 1H); 7.04-7.23 (m; 8H);

8.27 (t; *J* = 6.0 Hz; NHCO); 8.94 (s; 1H; OH); 10.47 (s; CONHO); $t_{R\ LCMS}$ 4.50 min; MS $(MH)^+$ *m/z* 335.

***N*-Benzyl-2-[1-(4-fluoro-phenyl)-meth-(Z)-ylidene]-*N*'-hydroxy-malonamide (10).** Beige powder; Yield 15%; Purity 99%; NMR ^1H (DMSO-d_6) δ ppm : 4.39 (d; *J* = 5.4 Hz; 2H); 7.22-7.36 (m; 7H); 7.44 (s; 1H); 7.56-7.60 (m; 2H); 8.23 (t; *J* = 5.4 Hz; NHCO); 9.15 (s; OH); 11.03 (s; CONHO); $t_{R\ LCMS}$ 4.17 min; MS $(MH)^+$ *m/z* 315.

***N*-(4-Fluoro-benzyl)-2-[1-(4-fluoro-phenyl)-meth-(Z)-ylidene]-*N*'-hydroxy-malonamide (11).** Beige powder; Yield 15%; Purity 95%; NMR ^1H (DMSO-d_6) δ ppm : 4.36 (d; *J* = 5.7 Hz; 2H); 7.12-7.36 (m; 6H); 7.43 (s; 1H); 7.56-7.60 (m; 2H); 8.27 (t; *J* = 5.7 Hz; NHCO); 9.14 (s; OH); 11.03 (s; CONHO); $t_{R\ LCMS}$ 4.36 min; MS $(MH)^+$ *m/z* 333.

2-Benzyl-*N*-(4-fluoro-benzyl)-*N'*-hydroxy-2-methyl-malonamide (12). White powder; Yield 60%; Purity 99%; NMR ^1H (CD_2Cl_2) δ ppm : 1.24 (s; 3H); 2.99 (s; 2H); 4.34 (s; 2H); 7.00-7.23 (m; 9H). $t_{R\ LCMS}$ 4.66 min; MS $(MH)^+$ *m/z* 331.

2-Benzyl-*N*-hydroxy-*N'*-pyridin-4-ylméthyl-malonamide (13). White powder; Yield 91%; Purity 99%; NMR ^1H (DMSO-d_6) δ ppm : 3.06-3.10 (m; 2H); 3.41 (t; *J* = 7.7 Hz; 1H); 4.47 (d; *J* = 5.7 Hz; 2H); 7.20-7.31 (m; 5H); 7.62 (d; *J* = 6.0 Hz; 2H); 8.63 (t; *J* = 5.7 Hz; CONH); 8.76 (d; *J* = 6.0 Hz; 2H); 10.64 (s; CONHO); $t_{R\ LCMS}$ 2.08 min; MS $(MH)^+$ *m/z* 300.

2-Benzylidene-*N*-hydroxy-*N'*-pyridin-4-ylmethyl-malonamide (14). White powder; Yield 90%; Purity 98%; NMR ^1H (DMSO-d_6) δ ppm : 4.58 (d; *J* = 5.7 Hz; 2H); 7.10-7.56 (m; 7H); 7.76 (s; 1H); 8.45-8.78 (m; 2H + NHCO); 11.09 (s; CONHO); $t_{R\ LCMS}$ 2.14 min; MS $(MH)^+$ *m/z* 298.

***Pf*AM1 inhibition.** Native *Pf*AM1 was purified according to the procedure described by Allary et al. [17], and diluted 10 times in Tris–HCl buffer (25 mM; pH 7.4) before use. The assays were set up in 96-well plates. The compounds were tested at the concentration of 10 µM. 33 µL of purified PfAM1 were pre-incubated 10 min at room temperature with 33 µL of

the inhibitor (30 µM in Tris–HCl buffer, 0.3% DMSO). 33 µL of the substrate Leu-pNA (Km = 0.099 mM) 0.3 mM in Tris–HCl buffer were then added. The reaction kinetics performed at room temperature was followed on a UV-microplate reader MultiskanRC (Labsystems, Finland) at 405 nm. The control activity was determined by incubating the enzyme in the same conditions without inhibitor. Bestatin was used as the reference inhibitor (IC_{50}=284 nM). The statistical Z' factor for the test was 0.82, allowing activities to be determined with a single point with a 95% confidence. Initial velocities are expressed in µmol. min^{-1}. Data were normalized to the controls that represent V_{max}. For the determination of IC_{50}s, initial velocities were plotted as a function of inhibitor concentration, using XLfit software from IDBS.

***p*APN inhibition**. Microsomal neutral aminopeptidase (APN) from porcine kidney was purchased from Sigma Inc. as an ammonium sulfate suspension (3.5 M $(NH_4)_2SO_4$ solution containing 10 mM $MgCl_2$) 10-40 units/mg protein. The enzyme suspension was diluted 600 fold in Tris–HCl buffer (25 mM; pH = 7.4) before use. The assays were performed in 96-well plates. The compounds were tested at the concentration of 10 µM. 33 µL of purified APN were pre-incubated 10 min at room temperature with 33 µL of the inhibitor (30 µM in Tris–HCl buffer, 0.3% DMSO). 33 µL of the substrate Leu-pNA (Km = 0.099 mM) 0.3 mM in Tris–HCl buffer were then added. The reaction kinetics performed at room temperature was followed on a UV-microplate reader MultiskanRC (Labsystems, Finland) at 405 nm. The control activity was determined by incubating the enzyme in the same conditions without inhibitor. Bestatin was used as the reference inhibitor (IC_{50} = 2.7 µM). The statistical Z' factor for the test was 0.75, allowing activities to be determined with a single point with a 95% confidence.[39] Initial velocities are expressed in µmol. min^{-1}. Data were normalized to the controls that represent V_{max}. For the determination of IC_{50}s, initial velocities were plotted as a function of inhibitor concentration, using XLfit software from IDBS.

In vitro P. falciparum **culture and drug assay.** Chloroquine-resistant *P. falciparum* 2/K 1-strain was cultured in human erythrocytes O^+ at 37 °C under a low oxygen atmosphere (3% O_2, 4% CO_2, and 93% N2) in RPMI-1640, supplemented with 10% human serum. Infected human red blood cells (200 µL, 1% parasitaemia, 2% haematocrit) were added to each well and incubated for 72 h. After incubation, test plates were frozen at −20 °C. Parasite multiplication was measured by the Malstat method. An amount of 100 µL of Malstat reagent was transferred to a new plate and mixed with 20 µL of the hemolysed parasite suspension for 15 min at room temperature. After addition of 20 µL of NBT/PES solution and 2 h of incubation in the dark, the absorbance was spectrophotometrically read at 655 nm (Biorad 3550 UV microplate reader). Percentage growth inhibition was calculated compared to the negative blanks. IC_{50} values are calculated from the duplicate determinations with relative difference below 25%.

Cytotoxicity test. MRC-5 SV2 cells, human fetal lung fibroblast, were cultivated in MEM, supplemented with L-glutamine (20 mM), 16.5 mM sodium hydrogen carbonate, and 5% FCS at 37 °C and 5% CO_2. For the assay, 10^4 MRC-5 cells/well were seeded onto the test plates containing the prediluted compounds and incubated at 37 °C and 5% CO_2 for 72 h. After 72 h of incubation, parasite growth was assessed fluorimetrically by adding resazurin for 24 h at 37 °C. Fluorescence was measured using a GENios Tecan fluorimeter (excitation 530 nm, emission 590 nm). IC_{50} values are calculated from duplicate determinations with relative difference below 25%.

LC-MS/MS analysis. The LC-MS/MS system consisted in a Varian 1200L (Varian, Les Ulis, France) a Prostar 430 autosampler, a (Varian, Les Ulis, France) triple quadrupole mass spectrometry equipped with an electrospray ionisation source, with a Prostar 325 detector. Analytes in incubation mixtures were separated by HPLC using a gelTSK C18 Super-ODS, 5 µm, 50 x 4.6 mm column (Interchim, Montluçon France). The mobile phase

solvents used were: (A) 0.01% formic acid in water; (B) 0.01% formic acid in acetonitrile. The following mobile phase gradient was applied: 0-100% (B) in 7.30min; hold at 100% (B) for 1min; 0-100% (A) in 0.30 min; 100% (A) hold for 10 min. The injection volume was 10 µL and the flow rate of 1 mL/min. Approximately 30% of the eluent was introduced into the triple quadrupole mass spectrometer source. The source temperature of the mass spectrometer was maintained at 300 °C, the declustering potential was 50 V, and the curtain gas pressure was 1.5 mTorr. Collision energy and observed transitions were respectively individually optimized for each compound (MRM mode).

Docking. The docking of BDM14471 in *PfAM1* (using PDB structure 3T8V) was performed using MOE 2009.10 software from Chem Computing Group.Inc. Briefly, the protein was prepared within the MOE package using Gasteiger partial charges, and the Generalized Born/Volume Integral Formalism for protonation at pH 7. The protein atoms were kept as rigid and the ligands as flexible. No restraints were used during docking (conformational search using MM Iteration Limit 1000; all other standard parameters were set on default) but the binding modes were chosen based on both the most favored predicted interaction energy with *Pf*AM1 and a proper chelating of the Zinc ion by the hydroxamic function.

Solubility. LogD. Plasma stability. a) Solubility: 40 µL of the 10 mM solution in DMSO of the sample were added to 1.960 mL of MeOH or PBS at pH = 7.4. The samples were gently shaked 24 h at room temperature, then centrifuged for 5 minutes and filtered over 0.45 µm filters. 20µL of each solution were added to 180 µL of MeOH and analyzed by LCMS-MS. The solubility was determined by the ratio of mass signal areas PBS /MeOH. b) Log D 40 µL of the 10 mM solution in DMSO of the sample were added to 1.960 mL of a 1/1 octanol / PBS at pH = 7.4 solution. The mixture was gently shaked 2 h at room temperature, then the two phases were separated. 20 µL of each solution was added to 180 µL of MeOH

and analysed by LCMS-MS. Log D was determined as the logarithm of the ratio of concentrations of product in octanol and PBS, determined by mass signals. c) Plasma stability. 40 µL of the 5 mM solution in DMSO of the sample were added to 1.960 mL of rat plasma (Male rat from Charles River Laboratories) to obtain a 100 µM final solution. The mixture was gently stirred 96 h at 37 °C. Aliquots of 200 µL were taken at various times (from 0 to 96 h) and diluted with 200 µL of phosphoric acid (0.14 M). 10 µL of the 2 mM solution in methanol of the internal standard were added. Compounds were extracted three times with 2 mL of AcOEt. The organic layer was evaporated, diluted with 200 µL of methanol and quantified by LCMS-MS, using a calibration curve.

Microsome stability. All chemicals were obtained from Sigma-Aldrich (Steinheim, Germany). Solvents were from common sources and of HPLC grade. Stock solutions of all compounds were prepared in methanol at a concentration of 0.1 mM. Pooled male mouse (CD-1) liver microsomes were purchased from BD gentest (Le Pont de Claix, France). All incubations were performed in duplicate in a shaking water bath at 37 °C. The incubation mixture were prepared in polypropylene tubes and contained 1 µM test compound (1% methanol), mouse liver microsomes (0.6 mg of microsomal protein / mL), 5 mM $MgCl_2$, 1 mM NADP, 5 mM glucose-6-phosphate, 0.4 U/mL glucose-6-phosphate dehydrogenase and 50 mM potassium phosphate buffer pH 7.4 in a final volume of 1.5 mL. Sampling points were taken at 5, 10, 15, 20, 25, 30, 45 and 60 min and reactions were terminated by adding ice-cold acetonitrile containing 1 µM internal standard (1 vol). The samples were centrifuged for 10 min at 4000 g, 4 °C to pellet precipitated microsomal protein, and the supernatant was subjected to LC-MS/MS analysis. Control incubations were performed with denaturated microsomes with acetonitrile containing 1 µM internal standard and sampling points were taken at 0 min and 60 min (to evaluate the compound chemical stability in the experimental conditions). Quantitation of each compound was achieved by conversion of the corresponding

analyte/internal standard peak area ratios in LCMS-MS (MRM mode) to percentage drug remaining, using the T0 ratio values as 100%. *In vitro* intrinsic clearance (CLint expressed as µl/min/mg) was calculated according to: Clint = (dose/AUC_{∞}), where dose is the initial amount of drug in the incubation mixture (1 µM) and AUC_{∞} is the area under the concentration versus time curve extrapolated to infinity. The slope of the linear regression from log percentage remaining versus incubation time relationships (-k) was used in the conversion to *in vitro* $T_{1/2}$ values by *in vitro* $T_{1/2}$ = -0.693/k.

GSH sensitivity. In a PP-tube of 1 mL are introduced 10 µL of a 10 µM-solution of compound in acetonitrile with 145 µL of phosphate buffer (0.067 M at pH = 7.4) and 145 µL of glutathione (5 mM/ H_2O).The final compound concentration is 330 µM. After 1 h of room-temperature incubation, samples are analyzed by LCMS to look for the glutathione conjugate.

***h*CA inhibition**[41] human-erythrocyte carbonic anhydrase activity was measured by following the reaction kinetics of hydrolysis of 4-nitrophenyl acetate (450 µM) on a UV-microplate reader at 400 nm, at CEREP,SA. The control activity was determined by incubating the enzyme in the same conditions without inhibitor. Acetazolamide (IC_{50} = 29 nM) was used as the reference inhibitor. The results are expressed as a percent inhibition of control specific activity (100 – ((measured specific activity/control specific activity) x 100)). This analysis was performed using a software developed at CEREP,SA.

Pharmacokinetic study[42] BDM14471 was formulated in 50/50 DMSO/PBS at 10 mg/mL and solubilized by short ultrasonic treatment (bath) if necessary. Twelve female CD-1 mice (approx. body weight 25-30 g) were given 1 x 50 mg/kg – single administration by intraperitonal injection and 2 mice for negative control (no treatment (blank plasma)). Food and drinking water remained available *ad libitum* throughout the trial. Blood samples (2 mice per data point) were collected at 15 min, 30 min, 1 h, 2 h, 4 h and 6 h. The blood was collected intracardially at the stated time point using a heparinized syringe (1 droplet – 2%

heparin) and transferred into an Eppendorf tube. The tubes were put on ice and centrifuged at 2600 rpm for 10 minutes to separate the plasma. The fractions of red cells or plasma were stored at 4 °C before analysis. Oasis®-HLB 1cc (30 mg) flangeless cartridges from Waters.Inc were activated with 1 mL methanol, then equilibrated with 1 mL water MilliQ. Samples were treated as follows. To 100 µL of plasma were added 2 µL of internal standard and 400 µL of water. To 100 µl of red blood cells were added 400 µL of water. The resulting suspension was sonicated and centrifuged; 400 µL of the supernatant were collected and 2 µL of internal standard were added. The resulting mixtures (from plasma or red blood cells) were eluted on an HLB-column. The column was then washed with 0.25 mL of water/MeOH (95/5 v/v). The compounds were eluted with a solution of acetonitrile/water (95/5 v/v) containing 0.1% of formic acid. The eluate was evaporated and re-dissolved in 200 µL of a methanol/mobile phase 60/40 (v/v) for LCMS-MS analysis.

ACKNOWLEDGMENTS

The authors thank Dr. N. Willand and B. Villemagne for their help with docking and visualization software. We are grateful to Inserm, Université de Lille2 and Institut Pasteur de Lille. This work was specifically funded by «Région Nord-Pas-de-Calais» and EC.

REFERENCES

(1) Nwaka, S.; Ramirez, B.; Brun, R.; Maes, L.; Douglas, F.; Ridley, R. Advancing Drug Innovation for Neglected Diseases - Criteria for Lead Progression. *PLoS Negl Trop Dis* **2009**, *3*, e440.

(2) Crowther, G. J.; Napuli, A. J.; Gilligan, J. H.; Gagaring, K.; Borboa, R.; Francek, C.; Chen, Z.; Dagostino, E. F.; Stockmyer, J. B.; Wang, Y.; Rodenbough, P. P.; Castaneda, L. J.; Leibly, D. J.; Bhandari, J.; Gelb, M. H.; Brinker, A.; Engels, I. H.; Taylor, J.; Chatterjee, A. K.; Fantauzzi, P.; Glynne, R. J.; Van Voorhis, W. C.; Kuhen, K. L. Identification of inhibitors

for putative malaria drug targets among novel antimalarial compounds. *Mol. Biochem. Parasitol.* **2011**, *175*, 21-29.

(3) Beghyn, T. B.; Charton, J.; Leroux, F.; Laconde, G.; Bourin, A.; Cos, P.; Maes, L.; Deprez, B. Drug to Genome to Drug: Discovery of New Antiplasmodial Compounds. *J. Med. Chem.* **2011**, *54*, 3222–3240.

(4) Beghyn, T. B.; Charton, J.; Leroux, F.; Henninot, A.; Reboule, I.; Cos, P.; Maes, L.; Deprez, B. Drug-to-Genome-to-Drug, Step 2: Reversing Selectivity in a Series of Antiplasmodial Compounds. *J. Med. Chem.* **2012**, *55*, 1274-1286.

(5) Blackman, M. J. Proteases involved in erythrocyte invasion by the malaria parasite: function and potential as chemotherapeutic targets. *Curr. Drug Targets* **2000**, *1*, 59-83.

(6) Blackman, M. J. Proteases in host cell invasion by the malaria parasite. *Cell. Microbiol.* **2004**, *6*, 893-903.

(7) Rosenthal, P. J. Hydrolysis of erythrocyte proteins by proteases of malaria parasites. *Curr. Opin. Hematol.* **2002**, *9*, 140-145.

(8) Wu, Y.; Wang, X.; Liu, X.; Wang, Y. Data-mining approaches reveal hidden families of proteases in the genome of malaria parasite. *Genome Res.* **2003**, *13*, 601-616.

(9) Drag, M.; Salvesen, G. S. Emerging principles in protease-based drug discovery. *Nat. Rev. Drug Discovery* **2010**, *9*, 690-701.

(10) Wegscheid-Gerlach, C.; Gerber, H.-D.; Diederich, W. E. Proteases of Plasmodium falciparum as Potential Drug Targets and Inhibitors Thereof. *Curr. Top. Med. Chem.* **2010**, *10*, 346-367.

(11) Murata, C. E.; Goldberg, D. E. Plasmodium falciparum falcilysin: a metalloprotease with dual specificity. *J. Biol. Chem.* **2003**, *278*, 38022-38028.

(12) Skinner-Adams, T. S.; Stack, C. M.; Trenholme, K. R.; Brown, C. L.; Grembecka, J.; Lowther, J.; Mucha, A.; Drag, M.; Kafarski, P.; McGowan, S.; Whisstock, J. C.; Gardiner, D.

L.; Dalton, J. P. Plasmodium falciparum neutral aminopeptidases: new targets for anti-malarials. *Trends Biochem. Sci.* **2009**, *35*, 53-61.

(13) Gardiner, D. L.; Skinner-Adams, T. S.; Brown, C. L.; Andrews, K. T.; Stack, C. M.; McCarthy, J. S.; Dalton, J. P.; Trenholme, K. R. Plasmodium falciparum: new molecular targets with potential for antimalarial drug development. *Expert Rev Anti Infect Ther* **2009**, *7*, 1087-1098.

(14) Gavigan, C. S.; Dalton, J. P.; Bell, A. The role of aminopeptidases in haemoglobin degradation in Plasmodium falciparum-infected erythrocytes. *Mol Biochem Parasitol* **2001**, *117*, 37-48.

(15) Gardiner, D. L.; Trenholme, K. R.; Skinner-Adams, T. S.; Stack, C. M.; Dalton, J. P. Overexpression of leucyl aminopeptidase in Plasmodium falciparum parasites. Target for the antimalarial activity of bestatin. *J. Biol. Chem.* **2006**, *281*, 1741-1745.

(16) Skinner-Adams, T. S.; Lowther, J.; Teuscher, F.; Stack, C. M.; Grembecka, J.; Mucha, A.; Kafarski, P.; Trenholme, K. R.; Dalton, J. P.; Gardiner, D. L. Identification of Phosphinate Dipeptide Analog Inhibitors Directed against the Plasmodium falciparum M17 Leucine Aminopeptidase as Lead Antimalarial Compounds. *J. Med. Chem.* **2007**, *50*, 6024–6031.

(17) Allary, M.; Schrevel, J.; Florent, I. Properties, stage-dependent expression and localization of Plasmodium falciparum M1 family zinc-aminopeptidase. *Parasitology* **2002**, *125*, 1-10.

(18) Florent, I.; Derhy, Z.; Allary, M.; Monsigny, M.; Mayer, R.; Schrevel, J. A Plasmodium falciparum aminopeptidase gene belonging to the M1 family of zinc-metallopeptidases is expressed in erythrocytic stages. *Mol Biochem Parasitol* **1998**, *97*, 149-160.

(19) Ragheb, D.; Dalal, S.; Bompiani, K. M.; Ray, W. K.; Klemba, M. Distribution and Biochemical Properties of an M1-family Aminopeptidase in Plasmodium falciparum Indicate a Role in Vacuolar Hemoglobin Catabolism. *J. Biol. Chem.* **2011**, *286*, 27255-27265.

(20) Klemba, M.; Gluzman, I.; Goldberg, D. E. A Plasmodium falciparum dipeptidyl aminopeptidase I participates in vacuolar hemoglobin degradation. *J. Biol. Chem.* **2004**, *279*, 43000-43007.

(21) Harbut, M. B.; Velmourougane, G.; Dalal, S.; Reiss, G.; Whisstock, J. C.; Onder, O.; Brisson, D.; McGowan, S.; Klemba, M.; Greenbaum, D. C. Bestatin-based chemical biology strategy reveals distinct roles for malaria M1- and M17-family aminopeptidases. *Proc. Natl. Acad. Sci. U.S.A.* **2011**, *108*, E526-E534.

(22) Kitjaroentham, A.; Suthiphongchai, T.; Wilairat, P. Effect of metalloprotease inhibitors on invasion of red blood cell by Plasmodium falciparum. *Acta Trop.* **2006**, *97*, 5-9.

(23) Azimzadeh, O.; Sow, C.; Geze, M.; Nyalwidhe, J.; Florent, I. Plasmodium falciparum PfA-M1 aminopeptidase is trafficked via the parasitophorous vacuole and marginally delivered to the food vacuole. *Malaria J.* **2010**, *9*, 189.

(24) Flipo, M.; Florent, I.; Grellier, P.; Sergheraert, C.; Deprez-Poulain, R. Design, synthesis and antimalarial activity of novel, quinoline-Based, zinc metallo-aminopeptidase inhibitors. *Bioorg. Med. Chem. Lett.* **2003**, *13*, 2659-2662.

(25) Flipo, M.; Beghyn, T.; Charton, J.; Leroux, V. A.; Deprez, B. P.; Deprez-Poulain, R. F. A library of novel hydroxamic acids targeting the metallo-protease family: design, parallel synthesis and screening. *Bioorg. Med. Chem.* **2007**, *15*, 63-76.

(26) Flipo, M.; Beghyn, T.; Leroux, V.; Florent, I.; Deprez, B. P.; Deprez-Poulain, R. F. Novel Selective Inhibitors of the Zinc Plasmodial Aminopeptidase PfA-M1 as Potential Antimalarial Agents. *J. Med. Chem.* **2007**, *50*, 1322-1334.

(27) Cunningham, E.; Drag, M.; Kafarski, P.; Bell, A. Chemical Target Validation Studies of Aminopeptidase in Malaria Parasites Using {alpha}-Aminoalkylphosphonate and Phosphonopeptide Inhibitors. *Antimicrob. Agents Chemother.* **2008**, *52*, 3221-3228.

(28) Velmourougane, G.; Harbut, M. B.; Dalal, S.; McGowan, S.; Oellig, C. A.; Meinhardt, N.; Whisstock, J. C.; Klemba, M.; Greenbaum, D. C. Synthesis of New (-)-Bestatin-Based Inhibitor Libraries Reveals a Novel Binding Mode in the S1 Pocket of the Essential Malaria M1 Metalloaminopeptidase. *J. Med. Chem.* **2011**, *54*, 1655-1666.

(29) McGowan, S.; Porter, C. J.; Lowther, J.; Stack, C. M.; Golding, S. J.; Skinner-Adams, T. S.; Trenholme, K. R.; Teuscher, F.; Donnelly, S. M.; Grembecka, J.; Mucha, A.; Kafarski, P.; DeGori, R.; Buckle, A. M.; Gardiner, D. L.; Whisstock, J. C.; Dalton, J. P. Structural basis for the inhibition of the essential Plasmodium falciparum M1 neutral aminopeptidase. *Proc. Natl. Acad. Sci. U.S.A.* **2009**, *106*, 2537-2542.

(30) Morgenthaler, M.; Aebi, J. D.; Grüninger, F.; Mona, D.; Wagner, B.; Kansy, M.; Diederich, F. A fluorine scan of non-peptidic inhibitors of neprilysin: Fluorophobic and fluorophilic regions in an enzyme active site. *J. Fluor. Chem.* **2008**, *129*, 852-865.

(31) Huang, Y.; Wolf, S.; Koes, D.; Popowicz, G. M.; Camacho, C. J.; Holak, T. A.; Dömling, A. Exhaustive Fluorine Scanning toward Potent p53–Mdm2 Antagonists. *ChemMedChem* **2012**, *7*, 49-52.

(32) Flipo, M.; Charton, J.; Hocine, A.; Dassonneville, S.; Deprez, B.; Deprez-Poulain, R. Hydroxamates: Relationships between Structure and Plasma Stability. *J. Med. Chem.* **2009**, *52*, 6790-6802.

(33) O'Hagan, D. Fluorine in health care: Organofluorine containing blockbuster drugs. *J. Fluor. Chem.* **2010**, *131*, 1071-1081.

(34) Gakh, A. A.; Burnett, M. N. Extreme modulation properties of aromatic fluorine. *J. Fluor. Chem.* **2011**, *132*, 88-93.

(35) Smart, B. E. Fluorine substituent effects (on bioactivity). *J. Fluor. Chem.* **2001**, *109*, 3-11.

(36) Saleh, M.; Abbott, S.; Perron, V.; Lauzon, C.; Penney, C.; Zacharie, B. Synthesis and antimicrobial activity of 2-fluorophenyl-4,6-disubstituted [1,3,5]triazines. *Bioorg. Med. Chem. Lett.* **2010**, *20*, 945-949.

(37) Bertrand, T.; Kothe, M.; Liu, J.; Dupuy, A.; Rak, A.; Berne, P. F.; Davis, S.; Gladysheva, T.; Valtre, C.; Crenne, J. Y.; Mathieu, M. The Crystal Structures of TrkA and TrkB Suggest Key Regions for Achieving Selective Inhibition. *J. Mol. Biol.* **2012**, 439-453.

(38) Whitehead, L.; Dobler, M. R.; Radetich, B.; Zhu, Y.; Atadja, P. W.; Claiborne, T.; Grob, J. E.; McRiner, A.; Pancost, M. R.; Patnaik, A.; Shao, W.; Shultz, M.; Tichkule, R.; Tommasi, R. A.; Vash, B.; Wang, P.; Stams, T. Human HDAC isoform selectivity achieved via exploitation of the acetate release channel with structurally unique small molecule inhibitors. *Bioorg. Med. Chem.* **2011**, *19*, 4626-4634.

(39) Kassahun, K.; Farrell, K.; Abbott, F. Identification and characterization of the glutathione and N-acetylcysteine conjugates of (E)-2-propyl-2,4-pentadienoic acid, a toxic metabolite of valproic acid, in rats and humans. *Drug Metab. Dispo.* **1991**, *19*, 525-535.

(40) Hasegawa, T.; Hara, K.; Hata, S. Binding of dorzolamide and its metabolite, N-deethylated dorzolamide, to human erythrocytes in vitro. *Drug Metab. Dispos.* **1994**, *22*, 377-382.

(41) Iyer, R.; Barrese, A. A.; Parakh, S.; Parker, C. N.; Tripp, B. C. Inhibition Profiling of Human Carbonic Anhydrase II by High-Throughput Screening of Structurally Diverse, Biologically Active Compounds. *J. Biomol. Screen.* **2006**, *11*, 782-791.

(42) Peng, S. X. Separation and identification methods for metalloproteinase inhibitors. *J Chromatogr B Biomed Sci App* **2001**, *764*, 59-80.

TOC Graphic:

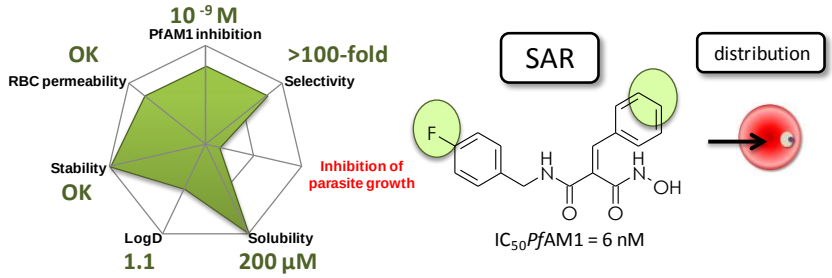
10 -9 M
PfAM1 inhibition
>100-fold
Selectivity
Solubility
200 µM
LogD
1.1
Stability
OK
RBC permeability
OK
Inhibition of
parasite growth
SAR
distribution
F
H
N
O
H
N
OH
O
IC50PfAM1 = 6 nM